Research Article

Monika Kroneberger* and Sebastian Fray

Scattering from reflective diffraction gratings: the challenges of measurement and simulation

https://doi.org/10.1515/aot-2017-0032
Received April 17, 2017; accepted August 8, 2017; previously published online September 11, 2017

Abstract: The accurate simulation of stray light is essential for the prediction of signal detection fidelity in an optical instrument with high contrast requirements. In a spectrometer, the scattering from reflective gratings is poorly understood and difficult to characterize, but contributes significantly to the overall system stray light and reduction in contrast. This paper describes the approaches that will be taken at OHB System AG to establish a sufficiently precise fitting of bidirectional scatter distribution functions (BSDFs) to existing data obtained from measurements of scattering from gratings. The work is being undertaken in preparation for the analysis and fitting of a BSDF to the scattering from the grating for the FLEX low-resolution spectrometer that will be measured in the second half of 2017.

Keywords: BSDF measurement; grating; scatter; spectrometer; stray light simulation.

1 Introduction

Specification of the scattering properties of gratings is often defined by comparison with the scatter due to micro-roughness of smooth reflecting surfaces. However, the surface roughness of the grating is only one contributor to the bidirectional scatter distribution functions (BSDF). Both grating structure and micro-structure due to the manufacturing process have a significant influence on the scattering characteristics of the grating. Measurements of the BSDF of gratings show a more-or-less Harvey-Shack scattering profile in the direction of the ruling, but enhanced scatter and multiple intensity levels of scatter depending on the scatter angle perpendicular to the ruling. This enhanced scattering is determined by the structure of the grating.

For stray light simulation, a BSDF model has to be found that reproduces the measured scattering pattern of the grating while not increasing simulation time excessively. Analytic functions are to be preferred to interpolation on tabulated measurement data because they are much faster, but the analytic functions have to represent the measured data well.

To determine the appropriate BSDF model for a grating, two major problems arise during the measurement of the pattern:

- Each measurement setup has a near-angle limit for the detection of the scattering signal in the proximity of the specular peak. This limits the characterization of the scatter close to the specular peak, which is often the most important contribution to signal degradation in optical systems;
- Not only one specular peak, but multiple diffraction peaks are observed in the measurements, and these peaks complicate the derivation of a BSDF model; they reduce the areas over which a straightforward analytical model for the measured signal can be found.

This paper describes the development of a computational tool for derivation of a BSDF from measurement data at OHB System AG. The development comprises both theoretical and experimental investigations. This paper presents the current status on theoretical analysis and verification of the measurement setup by modeling.

2 Measurement principle

For plane surfaces, the measurement of the BSDF can be easily performed with a light scattering measurement system. We will use the AlbatrossTT (http://www.iof.fraunhofer.de/content/dam/iof/en/documents/pb/en-Table-Top-Streulichtmesssystem-AlbatrossTT-TT.pdf) built by the Fraunhofer IOF.

***Corresponding author: Monika Kroneberger,** OHB Systems AG, Manfred-Fuchs-Str. 1, 82234 Wessling, Germany,
e-mail: monika.kroneberger@ohb.de.
http://orcid.org/0000-0002-4291-6418
Sebastian Fray: OHB Systems AG, Manfred-Fuchs-Str. 1, 82234 Wessling, Germany

www.degruyter.com/aot

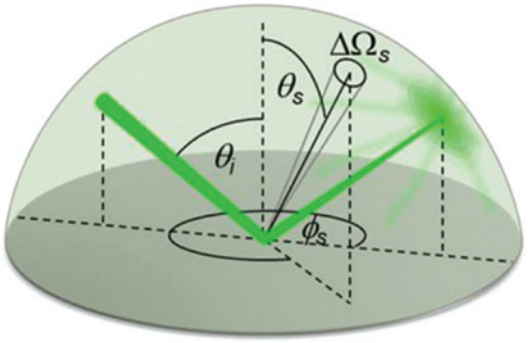

Figure 1: Principle of BSDF measurement.

The BSDF is calculated from measured data as follows:

$$\mathrm{BSDF}(\theta_i, \theta_s, \phi_s) = \frac{\Delta P_s(\theta_s, \phi_s)}{\Delta\Omega_s P_i \cos(\theta_s)}. \quad (1)$$

The index *i* refers to incident light, *s* to scattered light. The measurement principle is shown in Figure 1. P_i is the power incident on the sample and collected in the solid angle $\Delta\Omega_s$, respectively.

The intensity of the scattered light is measured by a movable detector. With the Albatross, the detector arm can sample almost the complete hemisphere (2D angular scan). For a simplified and shorter measurement, only a plane defined by incident and specular beam can be sampled (1D angular scan). An aperture in front of the detector determines the solid angle $\Delta\Omega_s$ within which the integrated intensity of the collected light is measured. The size of the aperture limits the angular resolution and the sensitivity of the measurement.

The incident light is focused onto the detector and normally has a spot size on the grating of roughly 2-mm diameter. The spot size on the sample determines the spatial resolution of the local topography. Larger spot sizes have the benefit of acquiring scatter properties averaged over a larger area. With small spot sizes, only local properties are characterized.

3 Measured BSDF and theoretical fit

In the early phases of optical development, a theoretical function for the scatter of optical surfaces is used for stray light simulations. For the surface roughness scatter, a Rayleigh-Rice model or the model developed by Wein [1] is used.

In these models, the scatter level is linked to a theoretical roughness value used for modeling all optical surfaces including gratings.

For the grating, this theoretical surface roughness does not represent a real surface roughness but a maximum scatter level allowed. This maximum allowed scatter level expressed in an equivalent surface roughness of a polished surface is called equivalent roughness of the grating in the following.

Harnisch et al. [2] measured a set of industry standard grating samples in 2012 to compare the results with the theoretical BSDF according to Wein [1].

In Figure 2, an example of one measured scatter distribution is shown. Besides the expected peaks and lower intensities for larger scatter angles, it shows multiple discrete scatter levels for different angular regimes.

The position and height of these discrete scatter levels is dependent on the grating production technology.

To assess the discrete scatter levels, Harnisch calculated theoretical scatter functions for multiple roughness values and overlaid them with the BSDF curve. Visual comparison showed the equivalent roughness of the grating.

Based on the Harnisch approach, we have developed a procedure for the processing of measured data to provide input to the simulation. We select the Harvey-Shack formula as a mathematical function to be used for a fit to the measured data. This will provide a worst case scenario due to the overestimation of the scatter in the direction perpendicular to the diffraction direction. An anisotropic model will be developed after verifying the isotropic approach.

The Harvey-Shack model uses three parameters and fits the measurement data by a log-log function: b_0 is the y-axis intersection, L is the roll over angle, and S is the slope of the descending part of the curve [equation (2)]. θ is the scatter angle, θ_0 the incident angle.

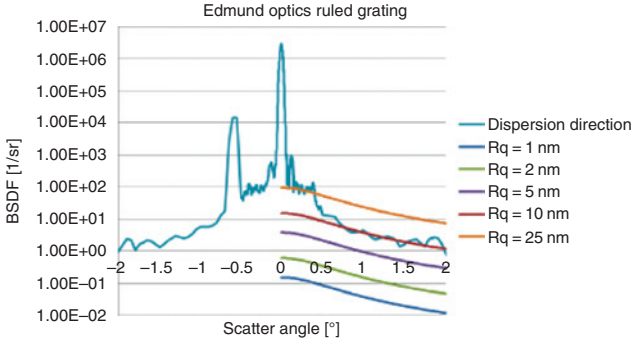

Figure 2: Measured BSDF from Harnisch et al. [2] with theoretical roughness BSDF perpendicular to the ruling. The main peak is the negative first diffraction order. The secondary peak is caused by a secondary wavelength produced by the source.

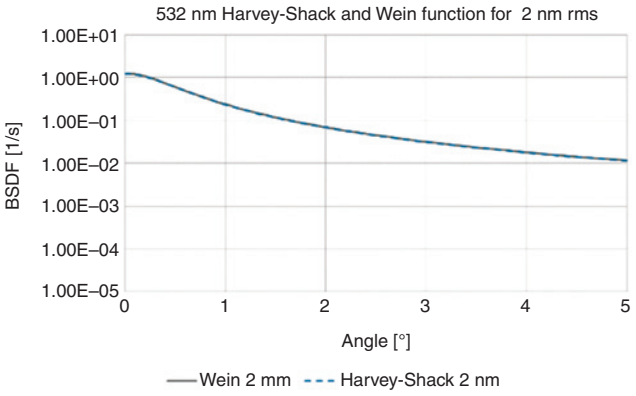

Figure 3: The Harvey-Shack function is a good theoretical function to fit to the theoretical roughness scatter function (5) mostly used in simulations and for requirement definitions.

$$\mathrm{BSDF}(\theta_i, \theta_s) = b_0 \left(1 + \left(\frac{\theta - \theta_0}{L} \right)^2 \right)^{S/2} \tag{2}$$

The characteristics of the Harvey-Shack function (see Figure 3) is almost identical to those of the roughness scatter function as used by Harnisch et al. [2] and depicted in Figure 2.

As seen in Figure 2, gratings can show scatter characteristics for which multiple functions are necessary to predict the scatter behavior. In this case, in particular, close to the diffraction peak, there is a step up in intensity of one order of magnitude. Therefore, multiple Harvey-Shack functions are needed to model the discrete steps in the scatter function.

To be able to do so, we developed a tool to fit multiple Harvey-Shack functions defined over local angular regions between the steps to measured BSDF data using standard python libraries. The final BSDF is the result of stitching the functions from each angular regime.

At the angles into which the light is diffracted and at the specular peak, the intensity of the direct light peak masks the scattered light (Figure 2). This defines the near-angle limit within which the scattered light cannot be determined.

The near-angle limit of a measurement is defined by the beam width and any aberration introduced by the sample. The minimum near-angle limit is a geometrical property of the system [see equation (3)]. The light is focused onto the detector, and a certain spot size on the sample is illuminated (see Figure 1).

$$\min \mathrm{NAL} = \tan^{-1} \left(\frac{r_{\mathrm{spot}}}{d_{s-d}} \right) \tag{3}$$

min NAL = minimum near angle limit,
r_{spot} = radius of spot on sample,
d_{s-d} = distance sample to detector

Any scattering in the system and any aberrations introduced add to this. This leads to additional difficulties while measuring gratings. The bandwidth of the source leads to a broadening of the diffraction peak. Curved gratings (such as the FLEX gratings) introduce additional optical power and aberrations broadening the peaks and making at least a refocusing of the system necessary. If no refocusing is applied, the near-angle limit will be enlarged by a few degrees rendering the measured scatter function unusable for simulation of high-resolution optical systems.

Another point of interest is the sampled area for the measurement. For plane and isotropic gratings, the point of incident of the light is of low relevance. For curved gratings, the point of intersection can be critical when the line spacing is not constant. Then, the measurement has to be done on the vertex of the grating to guarantee defined values for the line spacing. For any grating, the spot size of the incident light onto the grating must not be too small. The spot must illuminate a sufficient number of lines to create a representative diffraction pattern.

To obtain a sufficiently small spot size on the detector when measuring the scatter from a curved grating, the illumination system has to be refocused. This results in a smaller spot on the grating for convex gratings. Therefore, it is important to ensure that the refocusing does not result in a system configuration with a too small spot size on the grating.

Using the grating formula and the formula for calculating the resolution of a grating, the minimum number of illuminated lines can be evaluated by:

$$N = \frac{\lambda}{\sin(\varphi) g} \tag{4}$$

N: number of lines
g: grating constant
φ: angle to be resolved on detector

4 Theoretical implementation

To verify the described assumptions, a simplified optical model of the measurement setup was implemented in Zemax OpticStudio™ (Stansted, UK) and used to investigate various measurement configurations. The influence of the different configurations on the scattering predicted by the optical model can be evaluated. It can be decided if

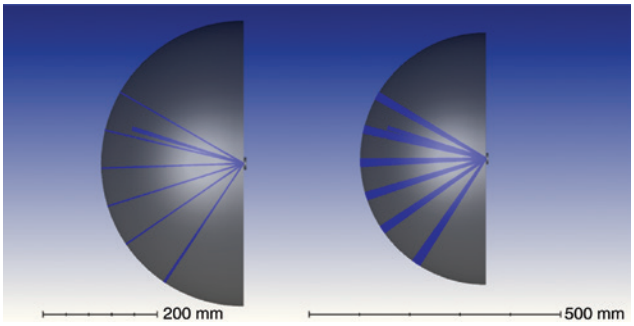

Figure 4: Raytrace of plane (left) and convex (right) grating with 500 lines/mm.

the model represents the measurement setup sufficiently accurately.

The model consists of an incoming beam with a spot size of 3 mm on the grating. After reflection from the grating, it is focused onto the detector hemisphere. For the grating diffraction, orders from –3 to +2 were simulated and, following Refs. [3] and [1], a 2-nm rms roughness scatter function of the form given in equation (5) was applied:

$$\mathrm{BSDF} = \frac{(\Delta n)^2}{8\pi} \cdot \frac{\left(\frac{2\pi}{\lambda}\right)^4 \sigma^2 L^2}{1 + \left(\frac{2\pi}{\lambda} L \sin\theta\right)^2} \tag{5}$$

$$L = 10^4 \text{ nm}, \sigma = \text{rms roughness}$$

Figure 4 shows the optical layout of the simplified measurement setup in Zemax without scattering. The locus of the moving detector is modeled by a hemispherical surface. On the left side, a plane grating is considered, while on the right side, it is a convex grating with a 100-mm radius. For the plane grating, the spots on the detector hemisphere are not aberrated, but for the convex grating, the beam becomes clearly unfocused by the curved sample.

Figure 5 shows the radiant intensity distributions on the detector sphere. The effective focal length of the system depends on the diffraction order. While the system is focused for the 0th order, consequently, the spot size of the other orders varies on the detector. For the convex grating, all diffraction orders are unfocused, and the spots are very large. This is in line with the expectations in Chapter 3. This optical model system is now used for further investigations.

The previously defined model of the measurement system will be optimized with regard to the relevant parameters. By refocusing and beam processing, the spot shall be reduced in size so that measurement as close as possible to the theoretical diffraction angle can be performed. The limiting angle is called the near-angle limit.

To investigate the influence of the curvature of the grating on the peak width, the simulated BSDF for the plane and the convex grating are compared in Figure 6.

In the normal configuration of the AlbatrossTT scatterometer (Fraunhofer IOF, Jena, Germany), the scatter function can only be measured down to 1.5° scatter angle. In high-resolution instruments like FLEX, this near-angle limit is not acceptable. Strict contrast requirements demand an accurate prediction of the stray light close to the geometric ray path.

In the theoretical system, refocusing is done with an ideal lens. In the real system, the illumination of the system is modified. This reduces the spot sizes on the detector significantly. The near-angle limit can be reduced to approximately 0.25° (see Figure 7), while still

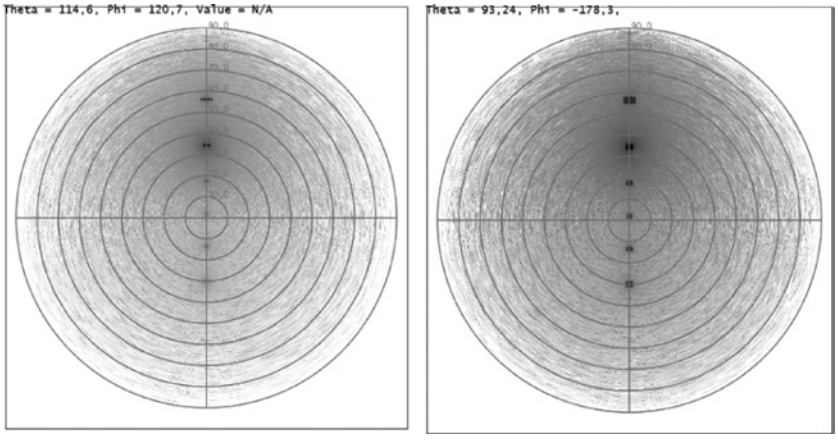

Figure 5: Radiant intensity distribution for plane (left) and convex (right) grating. Peaks are broader for the convex grating; focus is not on the detection sphere.

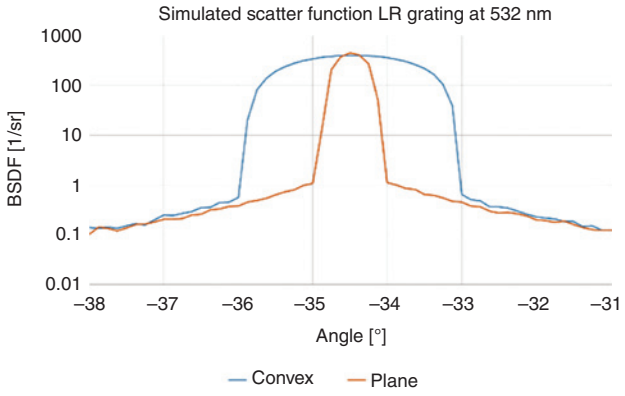

Figure 6: Nominal diffraction peak for plane and convex grating in normal AlbatrossTT configuration. Peak is enlarged by 2° for the convex grating.

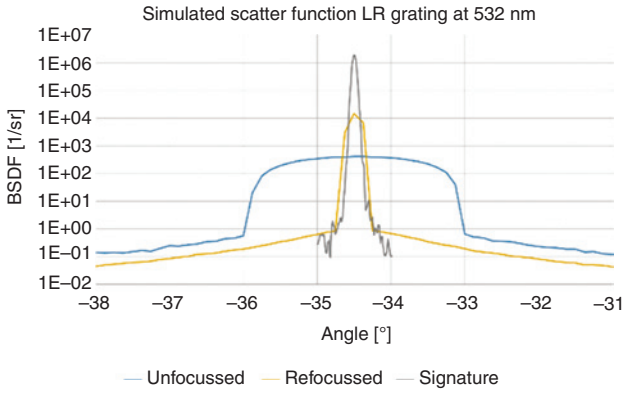

Figure 7: Nominal diffraction peak for convex grating in refocused AlbatrossTT configuration (unfocussed for comparison). Peak width is approximately 0.5°. Overlaid is the signature of the AlbatrossTT.

illuminating a spot on the grating with roughly 1-mm diameter (see Figure 8). With this spot size, at least 450 lines of the grating are illuminated. The diffraction pattern with this number of illuminated lines will be representative for the grating, and the diffraction peaks will not be enlarged by a too low number of illuminated patterns. According to equation (4), for a resolution of 0.1°, a minimum illuminated number of 152 lines are necessary.

In Figure 7, the instrument signature of the AlbatrossTT at OHB and the modeled BSDF of the measurement setup, including the convex grating, is overlaid. Comparing the curves in Figure 7 indicates that refocusing leads to a peak width (1/e width = 0.2°) that is almost as small as the system signature (1/e width = 0.1°).

The simulated minimum near-angle limit for the refocused system is 0.25° (measured as the point where the signature BSDF exceeds the grating BSDF). The theoretical model does not take into account the additional intrinsic limiting factors of the measurement setup. We use a Laser source, so assume a single wavelength. Additional wavelengths in the source would show as additional peaks or if close (in our case $\Delta\lambda \leqslant 10$ nm) to the original source wavelength, as broadening of the peak. The grating can introduce additional aberrations that would also lead to a broadening of the peaks.

However, to reduce the spot width by introducing a correction lens into an illumination system, to correct for the aberrations introduced by the grating is ineffective for a signature limited to 0.25°: aberrations and ghosts introduced by the lens outweigh any benefit. Therefore, for this paper, we continue with the simple refocused system.

5 Simulated BSDF and fit-to-roughness scatter

With the optimized model for the experimental setup, an appropriate modeling of the measurement data has

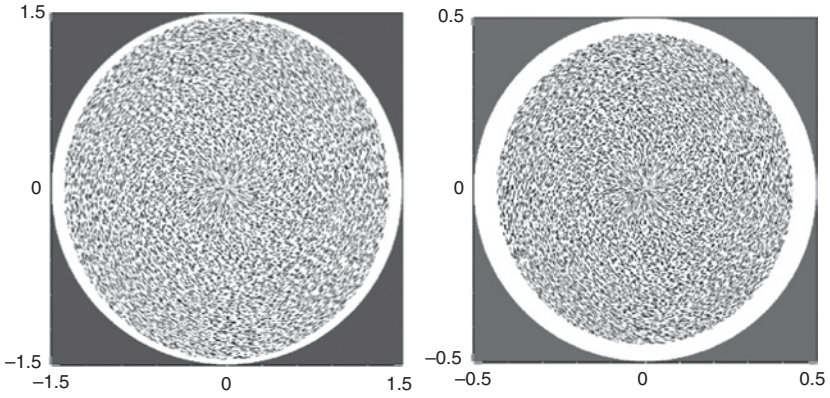

Figure 8: Illuminated spot at the grating surface in an unfocused (left) and a focused (right) system. The spot size is reduced from 3 mm to 0.9 mm in diameter.

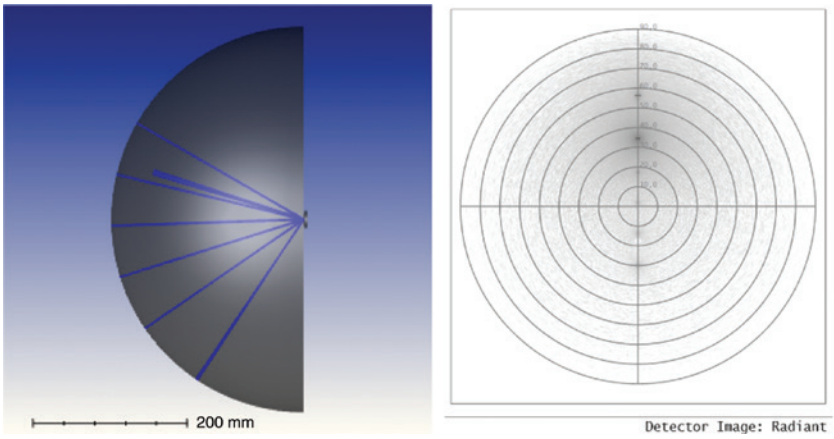

Figure 9: Refocused Zemax system and radiant intensity distribution with scatter for the FLEX LR grating.

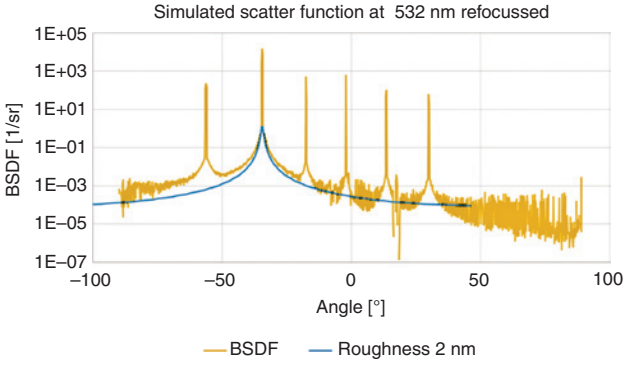

Figure 10: Simulated BSDF of the FLEX LR grating with theoretical roughness scatter BSDF.

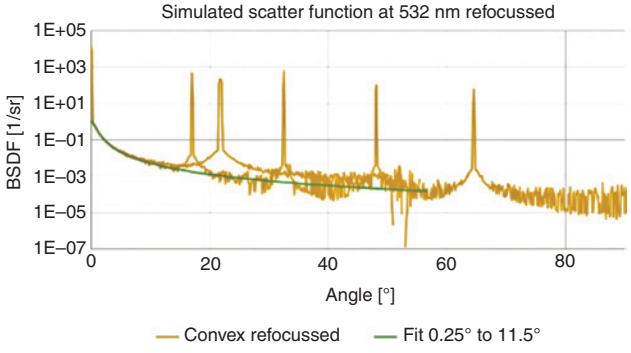

Figure 11: Simulated BSDF with fitted scatter function. Fit with one Harvey-Shack function.

been found. The modeled data is used to verify the fitting procedure.

Simulating the grating with scatter and detecting the angle-resolved power on the hemispherical surface results in a radiant intensity distribution (see Figure 9).

To analyze the scatter direction in the diffraction direction, the cross section through the diffraction plane was extracted. Figure 10 shows the simulated BSDF for 532 nm. The blue line is the theoretical roughness scatter BSDF that was used in the simulation for the grating surface.

In the FLEX LR system, only rays in an angular range in between the zeroth- and negative second-order diffraction reach the detector. Therefore, only the measured/simulated data inside the angular region between those two diffraction peaks are selected to fit a scatter function, i.e. scatter angles from 0.25° to 11.5° on both sides.

The resulting fitted function is in good agreement with the full simulated BSDF (see Figure 11).

The refocused system predicts the fitted BSDF with a precision sufficient for use as input to the stray light simulations.

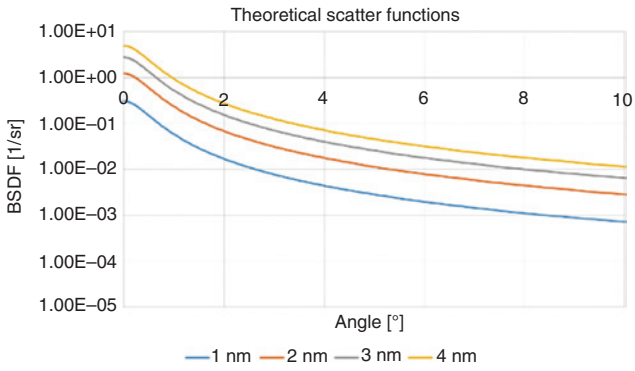

Figure 12: Theoretical scatter functions for 1- to 4-nm surface roughness at 532 nm. They build a family of curves shifted in the z axes.

The goal of the measurement is also to compare the scatter of the grating with the scatter of a polished surface. The requirement for the scatter characteristic of the FLEX LR grating is defined as an equivalent roughness of 2-nm rms surface roughness.

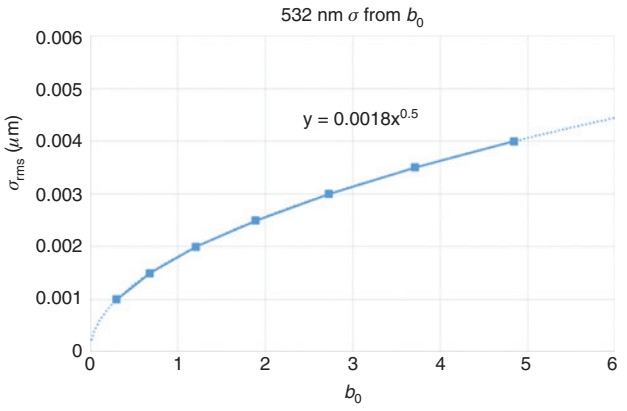

Figure 13: Dependency of surface roughness on the b_0 parameter of Harvey-Shack formula.

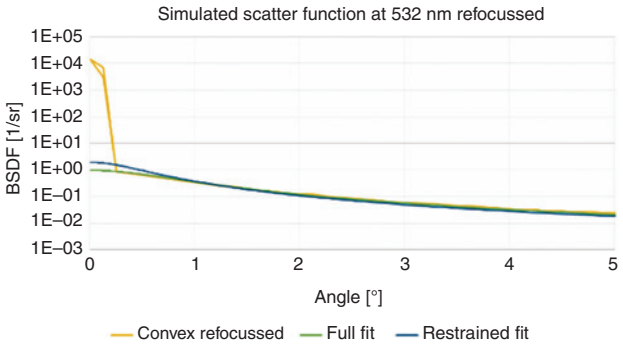

Figure 14: Fit to measured data for all three parameters and with fixed *L* and *S* values.

For the comparison of fitted to theoretical scatter functions, we calculate the family of curves for different surface roughness values according to equation (5). A fit to a single Harvey-Shack function is performed for each curve. Figure 12 shows the resulting BSDF. The functions are only displaced parallel to the BSDF axes.

With reference to equation (2) the displacement arises because only the b_0 value changes, while the *L* and *S* values stay constant. It must be taken into account that all parameters are dependent on the wavelength, as equation (5) shows a wavelength dependency.

A set of surface roughness calculations results in the following dependency of the value for surface roughness on b_0 at 532 nm (see Figure 13):

$$\sigma_{\text{rms}} = 0.0018 \cdot \sqrt{b_0}. \tag{6}$$

To extract the equivalent roughness value from measured data, the maximum stray light level must be fitted to a Harvey-Shack function with the *L* and *S* parameter fixed to the values calculated for the wavelength intended for measurement.

Figure 14 shows the resulting curve (constrained fit) overlaid to the simulated BSDF and the result of the fit considering all three parameters (full fit). The comparison with the full fit (Figure 11) shows less conformity with the measured data. Only for small angles, an increased scatter is predicted by the constrained fit. For higher angles, a good conformance can be achieved. This method allows a good derivation for a maximum roughness value.

The fitted b_0 value (1.93) is transferred into an equivalent surface roughness of 2.5 nm by equation (6). The BSDF used for simulation was based on 2-nm rms. This deviation is not only due to errors in the data but also to overlapping stray light from all diffraction orders. This overlay leads to a higher stray light for larger scatter angles and, thus, to an overestimation of the equivalent surface roughness.

6 Conclusion

In the course of analysis of the FLEX LR grating, OHB is developing a tool that allows for verification of stray light properties of complex grating structures.

The measured scatter function of the FLEX LR grating can be fitted with a theoretical function. The diffraction peaks have an angular distance allowing for sufficient data to fit to. A fit to one Harvey-Shack function is only feasible when the underlying scatter function is determined by a simple surface structure. More complex topologies resulting in multiple scatter levels like apparent on gratings can be handled by multiple Harvey-Shack functions.

As only simulated data instead of measured grating BSDF is available at this time, only a concept for our verification method could be investigated that has to be validated as soon as measured data is available.

However, by modeling data, it has been demonstrated how later experimentally recorded data could be compared with manufacturing requirements based on equivalent roughness.

This value must not be mistaken as a real surface roughness. It only allows a formulation of a requirement in terms of equivalent roughness.

Furthermore, the simulation shows that the fitted BSDF will overestimate the scatter level. This systematic deviation is caused by superposition of diffracted intensities of multiple orders.

We have shown that with appropriate modeling of the setup for scatter measurements, a sufficient reduction of the near-angle limit can be achieved, and the limits for optimization can be explored.

Acknowledgments: In the frame of FLEX development, OHB-Munich has run analyses on the FLEX LR assembly to investigate stray light from different sources. Results of this paper are partially based on this work that was funded by ESA through the FLEX Mission development program.

References

[1] S. J. Wein, PhD Theses University of Arizona (1989), 'Small-Angle Scatter Measurement'.
[2] B. Harnisch, A. Deep, R. Vink, C. Coatantiec, ICSO 2012, FP 156, 'Grating Scattering BSDF and Imaging Performances'.
[3] M. G. Dittman, Proc. SPIE 4774, 99–110 (2002).

Monika Kroneberger
OHB Systems AG, Manfred-Fuchs-Str. 1
82234 Wessling, Germany
monika.kroneberger@ohb.de

Monika Kroneberger received her diploma in Physics in 1991 from the Johann Wolfgang Goethe University in Frankfurt/Main. Currently, she is working in the domain of optical system engineering for OHB system AG. Her main topic is stray light reduction and verification in the optical systems by simulation and measurement.

Sebastian Fray
OHB Systems AG, Manfred-Fuchs-Str. 1
82234 Wessling, Germany

Sebastian Fray did his PhD thesis at the Max-Planck-Institute of Quantum Optics in Garching and received his PhD in Physics in 2004 from the Ludwigs-Maximilians Universität in Munich/Germany. Currently, he works at OHB System AG in the domain of optical system engineering involved in development of various optical space instruments for earth observation.